International Journal of Heat and Mass Transfer 53 (2010) 2703–2714

Contents lists available at ScienceDirect

International Journal of Heat and Mass Transfer

journal homepage: www.elsevier.com/locate/ijhmt

Vibration induced mixed convection in an open-ended obstructed cavity

Stephen Chung, Kambiz Vafai *

Department of Mechanical Engineering, University of California Riverside, Riverside, California, USA

ARTICLE INFO

Article history:
Received 29 November 2009
Received in revised form 14 January 2010
Accepted 14 January 2010

Keywords:
Mix convection
Vibration
Porous media
Open-ended cavity

ABSTRACT

Vibrational mixed convection inside an open-ended cavity filled with a porous medium is investigated in this work. Vertical vibration on the left wall and buoyancy induced flow are considered. The effect of variations in governing parameters, such as vibrational Reynolds number, modified Rayleigh number, and the Darcy number on streamlines, isotherms, and the average Nusselt number is discussed. Quantitative assessment and three dimensional qualitative mapping for vibrational, buoyancy, Darcian, and non-Darcian effects is obtained. It is found that vibrational effects are more pronounced at higher values of Darcy and Reynolds numbers, while buoyancy effects are dominant at lower values of Darcy and higher values of modified Rayleigh numbers. It is also found that Darcy and Regular fluid models are applicable at low and high values of Darcy number, respectively. At higher values of vibrational Reynolds and modified Rayleigh numbers, the generalized model should be used. The effect of variations of Prandtl number and dimensionless frequency are also examined in this work. Multiple validations show a very good agreement with some of the limited aspects of this study presented in previous works.

1. Introduction

Natural convection within the fluid-saturated porous medium has been studied extensively during the past decades [1–4]. This area is of interest due to a range of different applications, such as water movement in geothermal reservoirs, underground spread of waste, nuclear waste repository, and insulation engineering. Bejan and Tien [5] obtained an analytical solution for a porous layer with a horizontal end-to-end temperature difference. Their results were validated with experimental results, displaying a good agreement in the core area. The effect of the permeability of the end wall was also examined. Haajizadeh and Tien [6] studied the same problem with one permeable wall. Numerical, experimental, and asymptotic analytical solutions were obtained and compared with Bejan and Tien's [5] analytical solution.

Vafai and Tien [7] analyzed the effects of solid boundary and inertial forces on transport through porous media. Volume-averaging technique and matched asymptotic expansions were applied in developing the governing equations. Amiri and Vafai [8,9] have thoroughly investigated the effects of thermal non-equilibrium, inertial, boundary, variable porosity, and thermal dispersion on convection through a porous medium. They had characterized the importance of all of the pertinent parameters on the cited physical attributes.

Most of the works dealing with natural convection in porous media are based on an enclosure driven by a horizontal temperature gradient. However, it is important to consider open-ended enclosures since the interactions between the inside and outside domain of the enclosure can represent a number of fundamental and practical applications. Ettefagh and Vafai [10] and Ettefagh et al. [11] have investigated natural convection in obstructed open-ended cavities. The fundamentals of the physical attributes of open-ended and far field boundary conditions were discussed in Vafai and Ettefagh [12], Khanafer and Vafai [13], and Khanafer et al. [14].

A number of investigations [15–18] have discussed the vibrational convection. Vibrational convection can have some important applications. For example, Florio and Harnoy [17] had investigated the use of an oscillating plate to enhance the heat transfer from an obstacle located within an internal flow. Another example, relates to the effect of vibrational convection in space, where mechanically induced pseudo-gravity can be more significant due to a weak gravitational field [18].

The present work constitutes the first study of a vibration induced mixed convection in an open-ended obstructed cavity. A similar unobstructed configuration was investigated by Khaled and Vafai [19] earlier. They had examined vibrational and natural convection effects in an unobstructed vertical open-ended cavity. The purpose of this study is to understand the role of the porous medium on vibration induced mixed convection in an open-ended cavity. The significance of vibration, buoyancy, Darcian, and non-Darcian effects are discussed and thoroughly characterized for various physical conditions.

* Corresponding author. Tel.: +1 9518272135.
E-mail address: vafai@engr.ucr.edu (K. Vafai).

0017-9310/$ - see front matter © 2010 Elsevier Ltd. All rights reserved.
doi:10.1016/j.ijheatmasstransfer.2010.02.037

Nomenclature

Da	Dracy number
F	inertial coefficient
g	gravitational acceleration
H	height of the channel
K	permeability
Nu	Nusselt number
p	pressure
P	dimensionless pressure
Pr	Prandtl number
Ra	Rayleigh number
Ra_m	modified Rayleigh number
Re_s	vibrational Reynolds number
t	time
T	temperature
T_h	temperature of the vibrating wall
T_∞	environment temperature
u	horizontal velocity
$\vec{u}$	velocity vector
U	dimensionless horizontal velocity
v	vertical velocity
v_0	left wall's vertical vibrational velocity
V	dimensionless vertical velocity
W	width of the channel
x	horizontal coordinate
X	dimensionless horizontal coordinate
y	vertical coordinate
Y	dimensionless vertical coordinate
α	thermal diffusivity
β	thermal expansion coefficient
δ	porosity
ε	aspect ratio
θ	dimensionless temperature
γ	dimensionless vibration frequency
μ	dynamic viscosity
ν	kineimatic viscosity
ρ_f	fluid density at environmental temperature
σ	thermal capacitance ratio
τ	dimensionless time
τ^*	dimensionless time to reach harmonic status
ω	reference vibration frequency

Subscripts

eff	refers to effective property
Avg	refers to average amount
L	refers to the quantities which are evaluated at left wall

2. Formulation

The configuration analyzed in this work is shown in Fig. 1. A two dimensional vertical channel with fluid–saturated porous medium is considered. The channel has an open-end on the top and impermeable walls on the other three sides. The height of the channel is H which is significantly larger than its width W. The left wall has a uniform temperature T_h and vibrates vertically. The temperature of the right and bottom walls and the environment is T_∞ which is lower than T_h. The Boussinesq approximation is invoked and the vibration speed $v_0(t)$ is presented as:

$$v_0(t) = \omega H \sin(\gamma\omega t) \tag{1}$$

where ω is the reference frequency, γ, dimensionless frequency, and t is the time. The problem is considered as a transient, two dimensional, isotropic, homogeneous, laminar, and incompressible, with constant properties except for density where the Boussinesq approximation is invoked. The equations for conservation of mass, momentum, and energy are (Vafai and Tien [7] and Vafai [20]):

$$\nabla \cdot \vec{u} = 0 \tag{2}$$

$$\frac{\rho_f}{\delta}\frac{Du}{Dt} = -\frac{\partial p}{\partial x} + \mu_{eff}\nabla^2 u + -\frac{\mu_f}{K}u - \frac{\rho_f F\delta}{\sqrt{K}}u\sqrt{u^2+v^2} \tag{3a}$$

$$\frac{\rho_f}{\delta}\frac{Dv}{Dt} = -\frac{\partial p}{\partial y} + \mu_{eff}\nabla^2 v + \rho_f g\beta(T-T_\infty) - \frac{\mu_f}{K}v - \frac{\rho_f F\delta}{\sqrt{K}}v\sqrt{u^2+v^2} \tag{3b}$$

$$\sigma\frac{\partial T}{\partial t} + \vec{u}\cdot\nabla T = \alpha_{eff}\nabla^2 T \tag{4}$$

where u signifies the velocity in the x-direction and v signifies the velocity in the y-direction, p the pressure, T the temperature, ρ_f the density, β the thermal expansion coefficient, and μ_f is the dynamic fluid viscosity. The porous medium characteristics are described by δ the porosity, K the permeability, F the inertial coefficient of the porous media which depends on the Reynolds number and the microstructure, μ_{eff} the effective dynamic viscosity, α_{eff} the effective thermal diffusivity, and σ is the thermal capacitance ratio. It is assumed that μ_{eff} is the same as μ_f based on the works of Amiri and Vafai [8,9], Lundgren [21] and Neale and Nader [22]. The effect

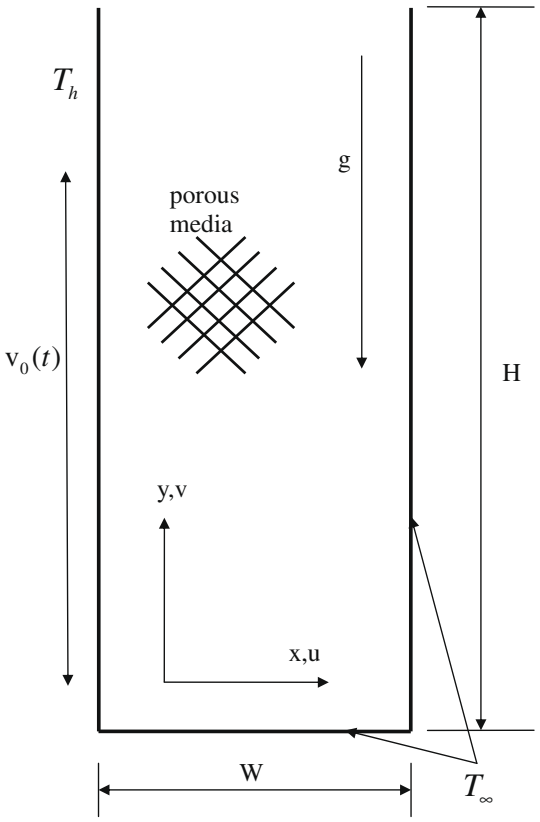

Fig. 1. Schematic of the configuration under investigation.

of thermal dispersion is incorporated in the effective thermal diffusivity.

2.1. Boundary and initial conditions

Initially, the entire domain is stationary and at the environment temperature T_∞, as given by:

$$u(x,y,0) = v(x,y,0) = 0; \quad T(x,y,0) = T_\infty \tag{5}$$

The vibrational condition at the left wall is described by:

$$u(0,y,t) = 0; \quad v(0,y,t) = \omega H \sin(\gamma\omega t); \quad T(0,y,t) = T_h \tag{6a}$$

The boundary conditions for the right and bottom walls are given by:

$$u(W,y,t) = v(W,y,t) = 0; \quad T(W,y,t) = T_\infty \tag{6b}$$

$$u(x,0,t) = v(x,0,t) = 0; \quad T(x,0,t) = T_\infty \tag{6c}$$

The boundary condition at the open-ended surface is given by:

$$\frac{\partial u}{\partial y}(x,H,t) = 0; \quad \frac{\partial T}{\partial y}(x,H,t) = 0 \tag{6d}$$

2.2. Dimensionless parameters and equations

For convenience, the equations are cast in dimensionless form by introducing the following dimensionless variables:

$$X = \frac{x}{W}; \quad Y = \frac{y}{H}; \quad U = \frac{u}{\omega H}; \quad V = \frac{v}{\omega H};$$
$$P = \frac{W^2 p}{\rho \upsilon^2}; \quad \theta = \frac{T - T_\infty}{T_h - T_\infty}; \quad \tau = \gamma\omega t; \tag{7}$$

This results in the following non-dimensional equations:

$$\varepsilon\frac{\partial U}{\partial X} + \frac{\partial V}{\partial Y} = 0 \tag{8}$$

$$\frac{\mathrm{Re}_s Da}{\delta}\left(\gamma\frac{\partial U}{\partial \tau} + \varepsilon U\frac{\partial U}{\partial X} + V\frac{\partial U}{\partial Y}\right) = -\frac{Da}{\mathrm{Re}_s\varepsilon}\frac{\partial P}{\partial X} + Da\left(\frac{\partial^2 U}{\partial X^2} + \frac{1}{\varepsilon^2}\frac{\partial^2 U}{\partial Y^2}\right) - U - \varepsilon F\delta\mathrm{Re}_s\sqrt{Da}U\sqrt{U^2+V^2} \tag{9a}$$

$$\frac{\mathrm{Re}_s Da}{\delta}\left(\gamma\frac{\partial V}{\partial \tau} + \varepsilon U\frac{\partial V}{\partial X} + V\frac{\partial V}{\partial Y}\right) = -\frac{Da}{\mathrm{Re}_s\varepsilon^2}\frac{\partial P}{\partial Y} + Da\left(\frac{\partial^2 V}{\partial X^2} + \frac{1}{\varepsilon^2}\frac{\partial^2 V}{\partial Y^2}\right) + \frac{Ra_m}{\varepsilon\mathrm{Pr}\mathrm{Re}_s}\theta - V - \varepsilon F\delta\mathrm{Re}_s\sqrt{Da}V\sqrt{U^2+V^2} \tag{9b}$$

$$\sigma\gamma\frac{\partial \theta}{\partial \tau} + \varepsilon U\frac{\partial \theta}{\partial X} + V\frac{\partial \theta}{\partial Y} = \frac{1}{\mathrm{Re}_s\mathrm{Pr}}\left(\frac{\partial^2 \theta}{\partial X^2} + \frac{1}{\varepsilon^2}\frac{\partial^2 \theta}{\partial Y^2}\right) \tag{10}$$

where $\mathrm{Re}_s = \frac{\omega W^2}{\upsilon}$ is the vibrational Reynolds number, $\mathrm{Pr} = \frac{\upsilon}{\alpha_{eff}}$ Prandtl number, $Da = \frac{K}{W^2}$ Darcy number, $Ra_m = Ra \cdot Da = \frac{\beta g K W \Delta T}{\alpha_{eff}\upsilon}$ modified Rayleigh number where $Ra = \frac{\beta g W^3 \Delta T}{\alpha_{eff}\upsilon}$ is the regular Rayleigh number, and $\varepsilon = \frac{H}{W}$ is the aspect ratio. The relationship obtained by Beavers and Sparrow [23] expressed by $F\delta = 0.074$ is applied in this study to evaluate the geometric shape parameter, F. The porosity and aspect ratio are $\delta = 0.9$ and $\varepsilon = 4$, respectively.

The dimensionless boundary and initial conditions can be presented as:

$$U(X,Y,0) = V(X,Y,0) = \theta(X,Y,0) = 0 \tag{11}$$

$$U(0,Y,\tau) = 0; \quad V(0,Y,\tau) = \sin(\tau); \quad \theta(0,Y,\tau) = 1 \tag{12a}$$

$$U(1,Y,\tau) = V(1,Y,\tau) = \theta(1,Y,\tau) = 0 \tag{12b}$$

$$U(X,0,\tau) = V(X,0,\tau) = \theta(X,0,\tau) = 0 \tag{12c}$$

$$\frac{\partial U}{\partial Y}(X,1,\tau) = \frac{\partial \theta}{\partial Y}(X,1,\tau) = 0 \tag{12d}$$

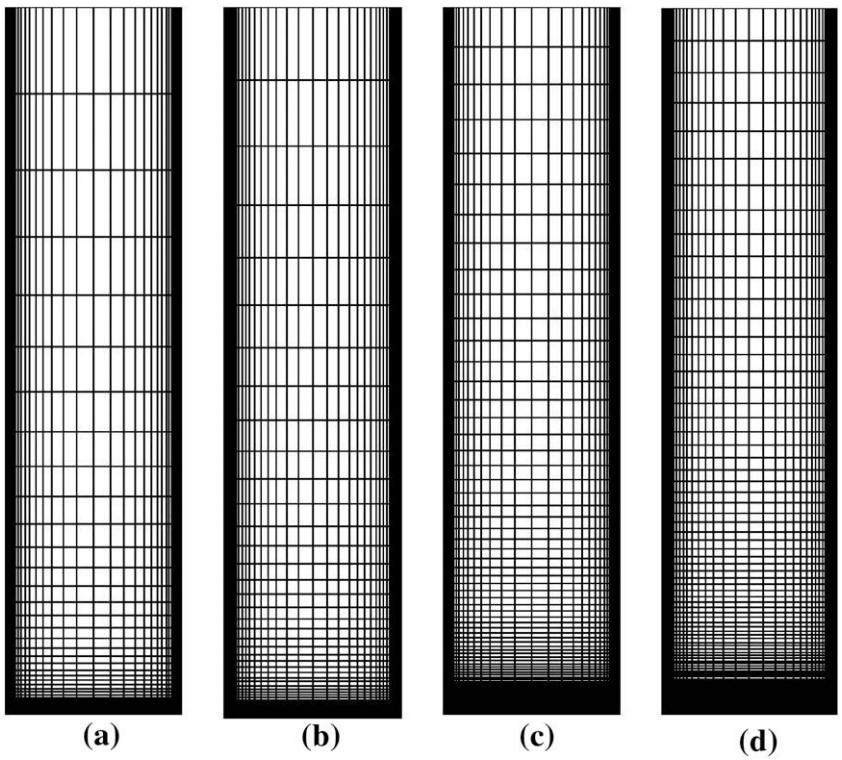

Fig. 2. Element distribution for (a) Mesh 1, (b) Mesh 2, (c) Mesh 3, (d) Mesh 4.

Table 1
Four sets of mesh distributions which were utilized in the present investigation.

Mesh	Elements number in *X*-direction	Elements number in *Y*-direction	Size ratio in *X*-direction	Size ratio in *Y*-direction
1	50	50	150	600
2	60	60	150	600
3	50	100	150	300
4	60	120	150	300

2.3. Measure of the thermal response

The Nusselt number on the left wall which is used as a measure to characterize the thermal response of the system is defined as:

$$Nu_L(Y,\tau) \equiv \frac{hW}{k} = \frac{1}{1-\theta_{Avg}(Y,\tau)} \frac{\partial\theta(0,Y,\tau)}{\partial X} \tag{13}$$

where h is the local convection coefficient at the left wall and k is the thermal conductivity of the fluid. The local average temperature difference θ_{Avg} at a Y cross section is defined as:

$$\theta_{Avg}(Y,\tau) = \int_0^1 \theta(X,Y,\tau)dX \tag{14}$$

The average Nusselt number of the left wall is defined as:

$$Nu_{Avg} = \int_{\tau^*}^{\tau^*+2\pi} \int_0^1 Nu_L(Y,\tau)dY\,d\tau \tag{15}$$

where τ^* is dimensionless time to reach the harmonic status. Nu_{Avg} represents the heat transfer on the vibrating left wall and is used as a parameter which characterizes the thermal response of the system.

Table 2
Pertinent cases studied in this investigation: cases 1–7 were based on using mesh 1 and the critical cases 8–14 were based on mesh 3.

Case	Re_s	Ra_m	Da
1	1000	1000	10^{-2}
2	1000	100	10^{-6}
3	1000	100	10^{-2}
4	100	1000	10^{-2}
5	100	1000	1
6	Darcy model	100	Darcy model
7	100	Regular fluid model $Ra = 10^6$	Regular fluid model
8	1000	1000	$Da = 10^{-6}$
9	1000	1000	$Da = 10^{-5}$
10	1000	1000	$Da = 10^{-4}$
11	1000	1000	$Da = 10^{-1}$
12	1000	1000	$Da = 1$
13	Darcy model	1000	Darcy model
14	1000	Regular fluid model $Ra = 10^6$	Regular fluid model

3. Numerical methodology

The results for this study were mainly obtained by using Comsol Multiphysics software. COMSOL uses the finite element method with adaptive meshing and error control with various numerical solvers. The solver is set as a time-dependent solver with a direct linear system solver UMFPACK. The time-dependent solver is set with an initial time step as 5×10^{-7}% of one time period, 2π, and maximum time step as 0.5% of 2π.

The non-uniformly distributed grid distribution used in this work is shown in Fig. 2. Mesh distribution is developed and controlled by the number of elements and the size ratio as shown in Fig. 2. Size ratio is defined as the ratio of the length between the

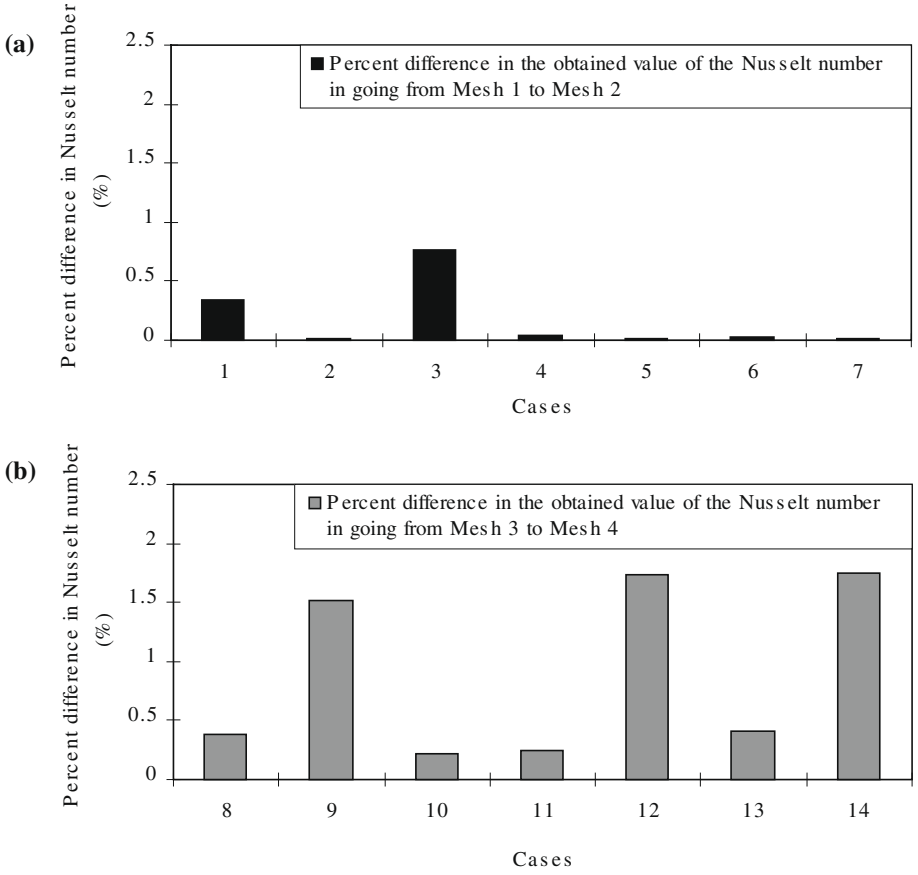

Fig. 3. Percent difference in the obtained value of the Nusselt number in going from (a) Mesh 1 to Mesh 2; (b) Mesh 3 to Mesh 4.

Table 3
Validation of Forchheimer-extended Darcy flow component of the current study and those by Ettefagh et al. [11], Prasad and Tutomo [1] and Lauriat and Prasad [24] for natural convection within an enclosure.

A	∞	55	11	5.5	1.1	0.55	0.11	0.05
Fs/Pr^*	0	10^{-4}	5×10^{-4}	10^{-3}	5×10^{-3}	10^{-2}	5×10^{-2}	10^{-1}
	Nu							
Present work	8.93	8.84	8.55	8.26	7.02	6.29	4.46	3.73
Ettefagh et al. [11]	8.98	8.92	8.67	8.44	7.24	6.46	4.55	3.8
Prasad and Tutomo [1]	9.27	9.17	8.84	8.52	7.51	6.36	4.67	3.87
Lauriat and Prasad [24]	8.96	8.9	8.6	8.45	7.31	6.56	4.6	3.82
$Ra_m = 500$	$A = 1$	Pr = 1	Forchheimer-extended Darcy flow model					

largest and smallest elements. Four sets of mesh distributions were investigated in this study, as shown in Table 1 and displayed in Fig. 2. Mesh 1 is applied for most of the simulations as it produces less than 0.7% difference compared to when mesh 2 is utilized as shown in Fig. 3a. For a subset of computational simulations shown in Table 2, cases 8–14, a more refined mesh distribution, mesh 3, was utilized. Comparing the differences between mesh 3 and mesh 4, as shown in Fig. 3b, it can be seen that mesh 3 distribution can be used for this subset of computational runs.

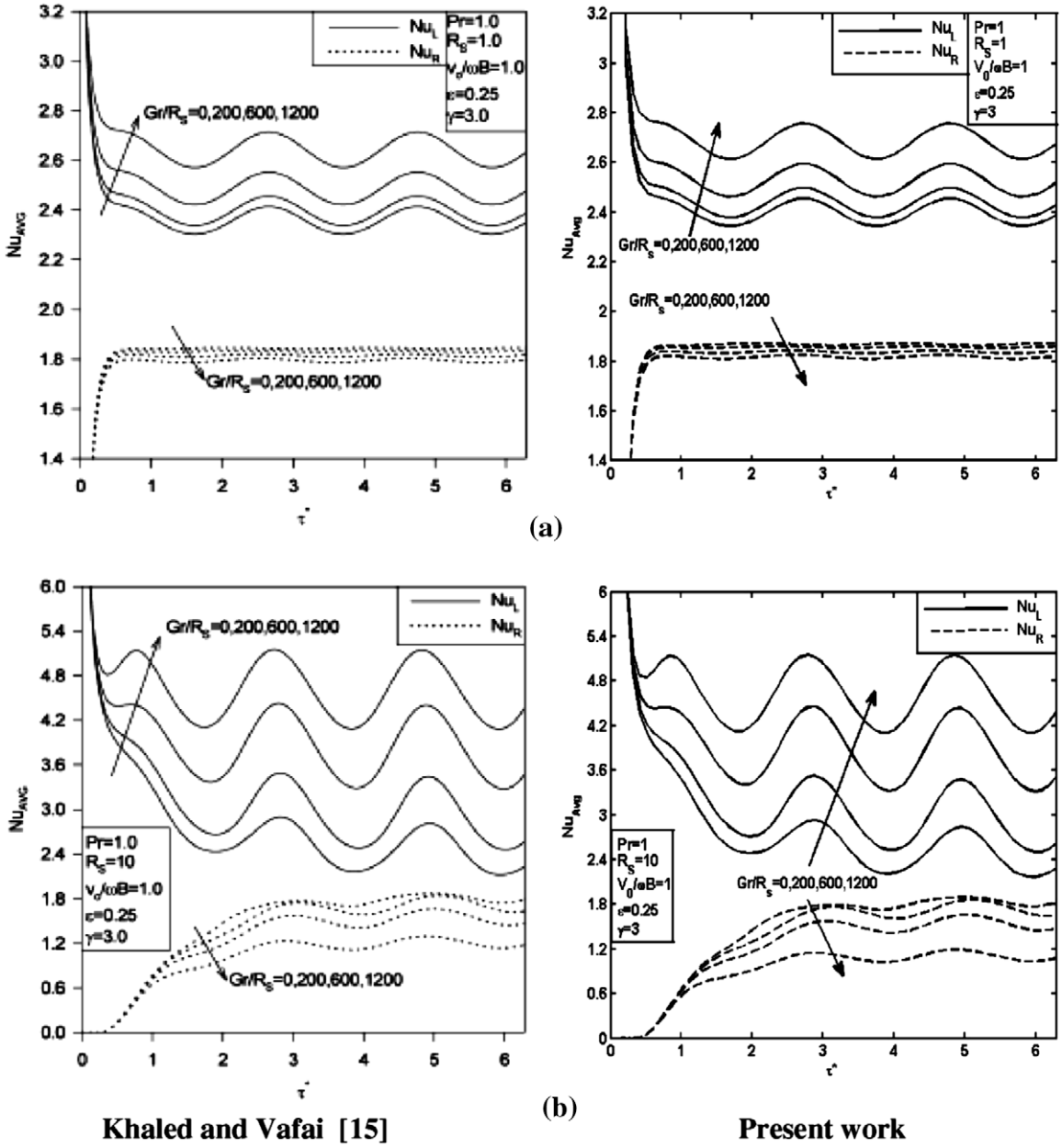

Fig. 4. Comparison of temporal Nusselt number distribution at different Grashof and vibrational Reynolds number on both walls with those by Khaled and Vafai [15].

Table 4
Validation of the Brinkman-extended Darcy flow component of the current work with studies by Ettefagh at al. [11] and Prasad et al. [25].

Da	10^{-5}	10^{-5}	10^{-5}	10^{-3}	10^{-3}	10^{-3}
Ra_m	10	100	1000	10	100	1000
	Nu					
Present	1.076	3.026	12.32	1.05	2.42	7.17
Ettefagh et al. [11]	1.09	3.06	12.64	1.06	2.45	7.42
Prasad et al. [25]	1.07	3.02	12.42	1.05	2.41	7.29
	$A = 1$	Pr = 1	Brinkman-extended Darcy flow model			

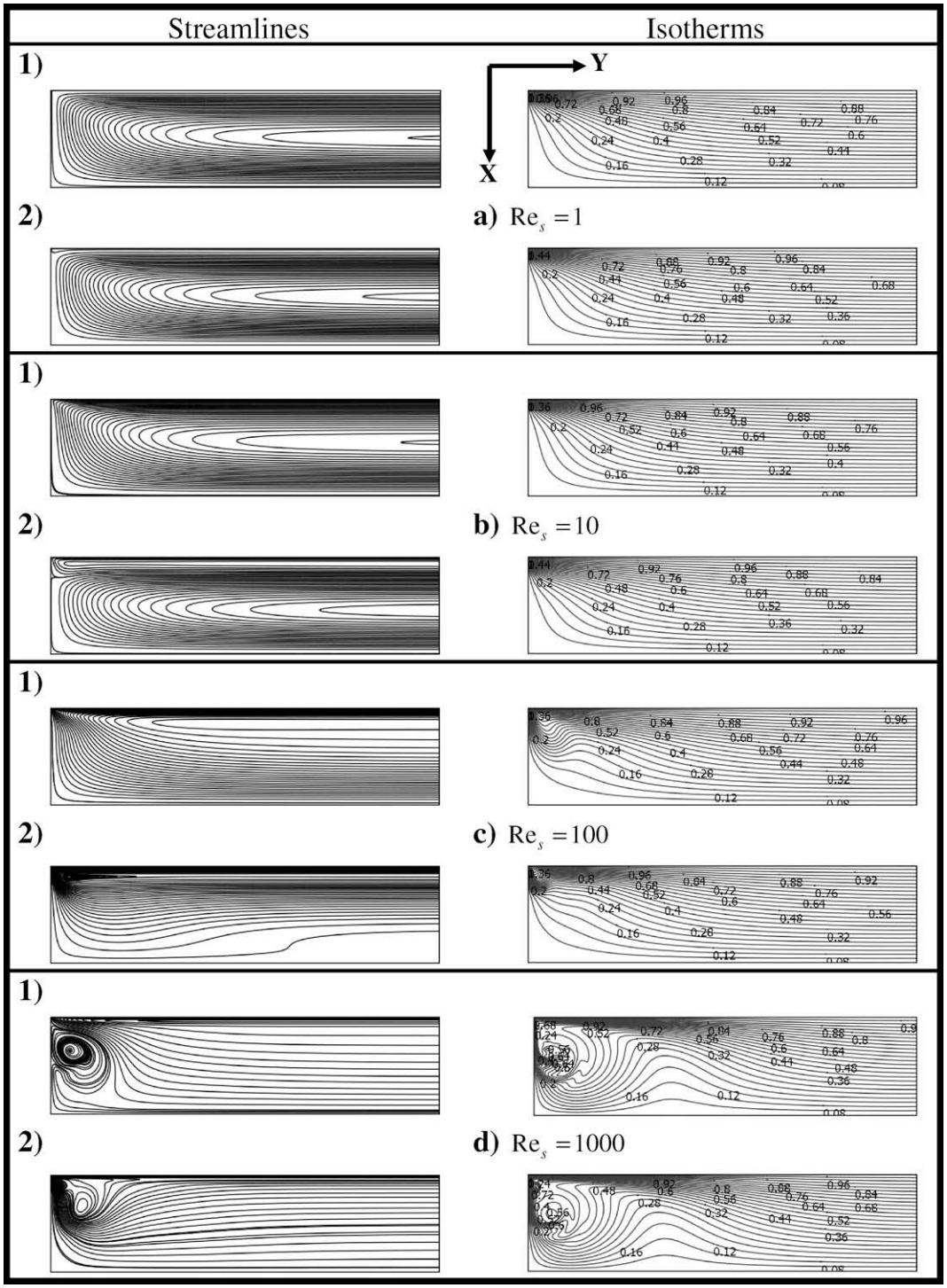

Fig. 5. Effects of variations in the vibrational Reynolds number on the streamlines and isotherms for Pr = 1, $\gamma = 3$, $Ra_m = 1000$, $Da = 10^{-2}$, $\delta = 0.9$, $\sigma = 1$, $\varepsilon = 4$ for two time steps at Re_s = 1, 10, 100, 1000 (a–d).

4. Validation and comparison

The results obtained from the current work are validated against the previous works related to vibrational mixed convection, Forchheimer-extended, and also Brinkman-extended Darcy models. For validation of vibrational mixed convection, there are no studies that have investigated the presence of a porous medium. The current work constitutes the first of such studies. The work on buoyancy and vibration induced flow within an open-ended channel by Khaled and Vafai [15] is used as one of the sources of comparisons. Temporal Nusselt number distribution at different Grashof and vibrational Reynolds numbers on both walls are compared against the work of Khaled and Vafai [15] as shown in Fig. 4. As can be seen the results are in very good agreement.

For validation of Forchheimer-extended Darcy flow model, the results for a rectangular enclosure are compared against those by Prasad and Tuntomo [1], Ettefagh et al. [11], and Lauriat and Prasad

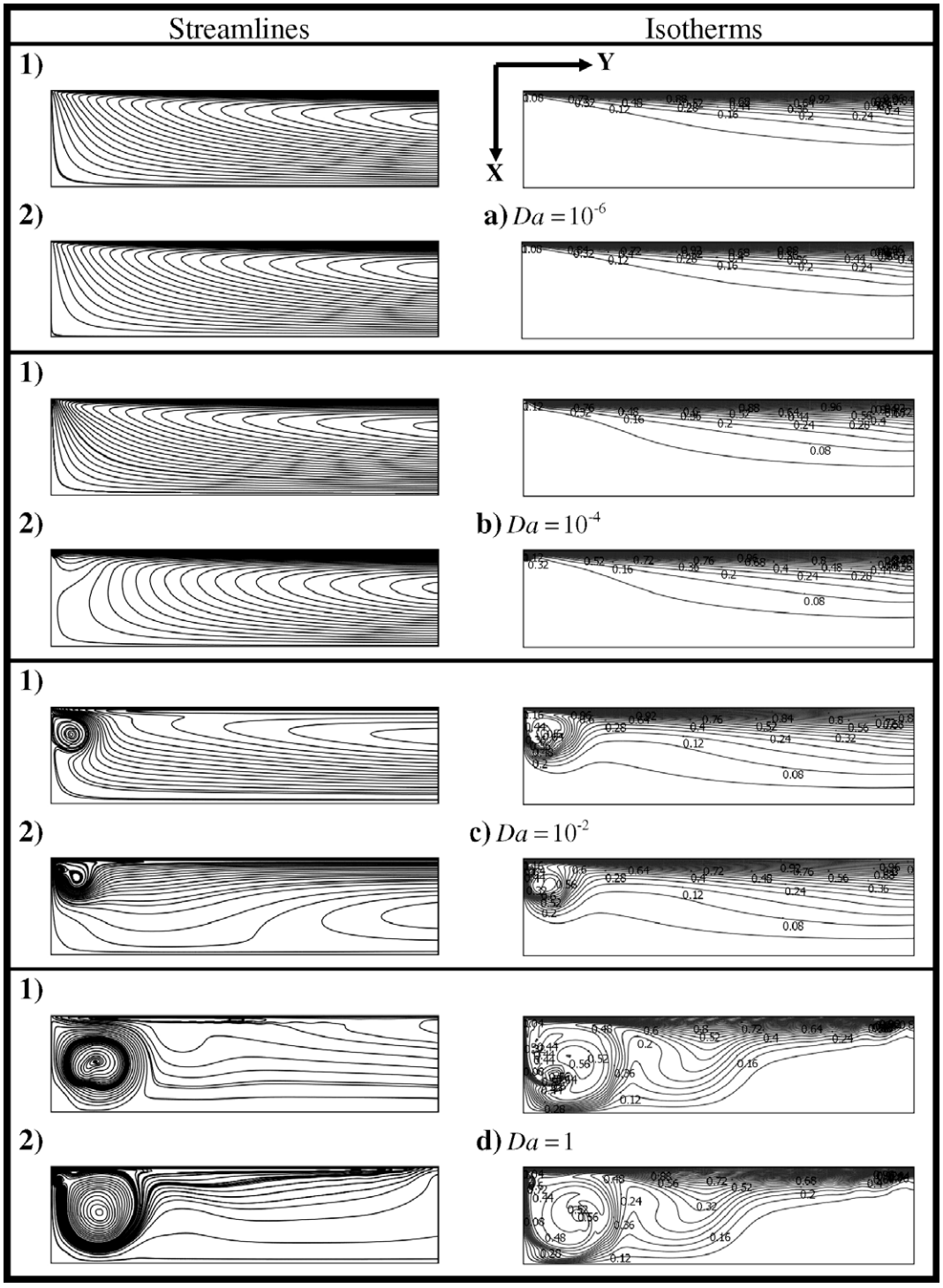

Fig. 6. Effect of the obstructing medium on the streamlines and Isotherms for Pr = 1, $\gamma = 3$, $Ra_m = 1000$, $Re_s = 1000$, $\delta = 0.9$, $\sigma = 1$, $\varepsilon = 4$ for two time steps at $Da = 10^{-6}$, 10^{-4}, 10^{-2}, 1 (a–d).

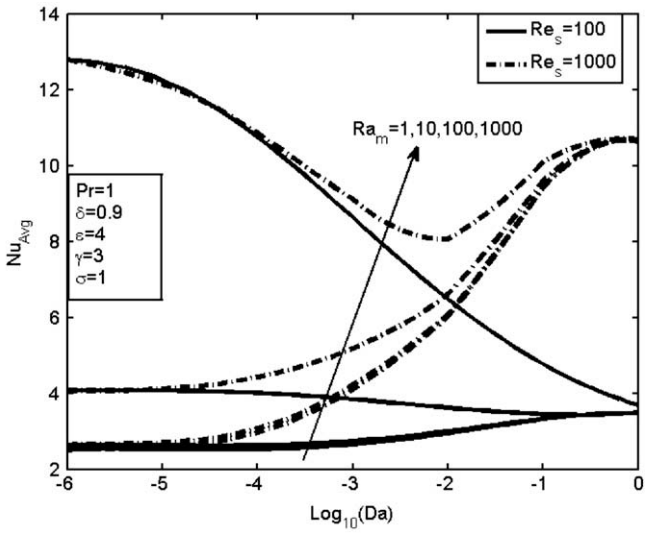

Fig. 7. Effect of variations Re_s, Ra_m, and Da on the average Nusselt number, Nu_{Avg}.

[24]. The Forchheimer's term is expressed as $\frac{\rho F\delta}{\sqrt{K}}\sqrt{u^2+v^2}(u\hat{i}+v\hat{j})$ and $F\delta = 0.074$. The comparisons are done at various values of inertial parameter Λ and Forchheimer number divided by the Prandtl number Fs/Pr^*. As can be seen in Table 3, the results are in very good agreement with the results of Ettefagh et al. [11].

An additional validation is presented for Brinkman-extended Darcy flow model. In Table 4, the results from the present work are compared against those given in Ettefagh et al. [11], and Prasad et al.'s [25] works. The results are compared against a range of modified Rayleigh, Ra_m and Darcy, Da numbers. Again a very good agreement is observed.

5. Result and discussion

5.1. Vibrational effects

Fig. 5 shows the effect of variations in the vibrational Reynolds number Re_s (1–1000) on the streamlines and the isotherms. It should be noted that time step 1 ($\tau = \tau^* + 3/2\pi$) is the time it takes for the left wall to move up while aligned with the buoyancy force and the time step 2 ($\tau = \tau^* + 11/6\pi$) is the time it takes for the left wall to move downward against the direction of the buoyancy force. As Re_s increases from 1 (Fig. 5a), a vibrational induced flow layer forms at the left wall during time step 2 which gradually replaces the buoyancy induced flow layer at larger values of Re_s and eventually (Fig. 5d with $Re_s = 1000$) occupies the whole domain. It can also be seen that in the lower portion of the channel, at higher values of Re_s, the vibrational induced flow changes from reciprocating motion to a rotating motion.

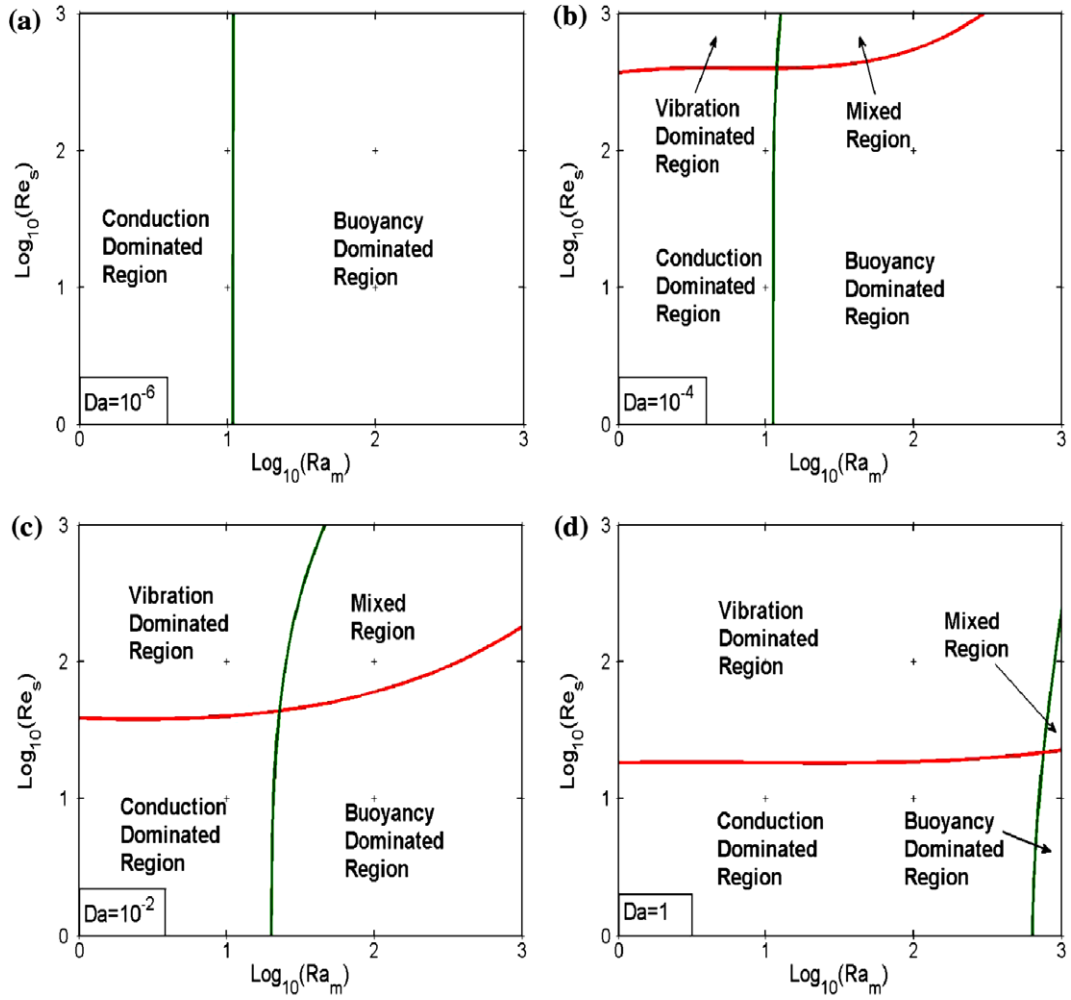

Fig. 8. Quantitative assessment of different flow regimes based on variations in Re_s, Ra_m, and Da (Pr = 1, $\gamma = 3$, $\delta = 0.9$, $\sigma = 1$, $\varepsilon = 4$).

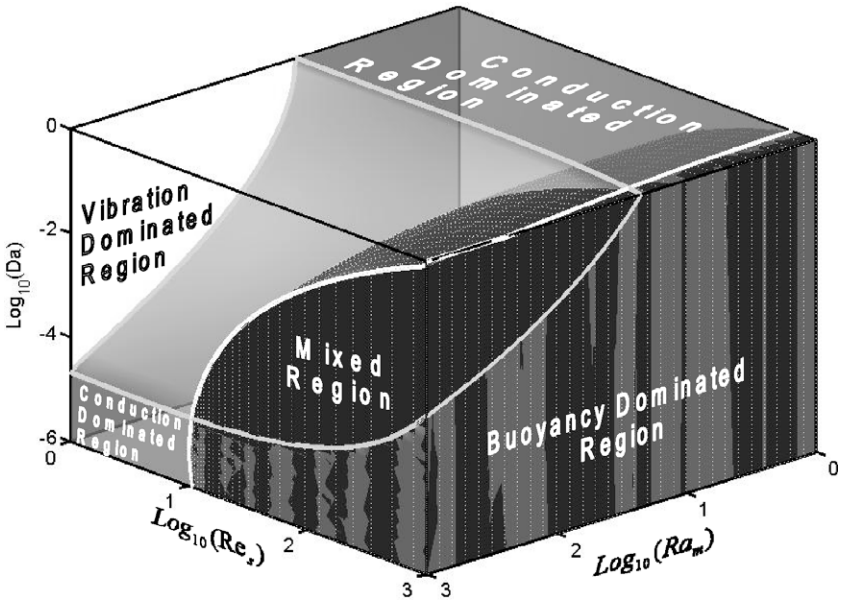

Fig. 9. Three dimensional qualitative mapping of different flow regimes based on variations in Re_s, Ra_m, and Da (Pr = 1, $\gamma = 3$, $\delta = 0.9$, $\sigma = 1$, $\varepsilon = 4$).

At lower values of Re_s (Fig. 5a and b with $Re_s = 1$ and 10), the dominant mode of heat transfer is by conduction, which is not much affected by either buoyancy or vibration. At higher values of Re_s a thermally stratified flow with a thinner thermal boundary layer starts forming along the bottom portion of the channel. As can be seen in Fig. 5, the rotating motion appears to induce an enhanced heat transfer between the hot and cold walls. This reciprocating motion can have either an enhancing or suppressive effect on the heat transfer across the channel.

5.2. Effect of the obstructing medium

Fig. 6 illustrates the effect of the obstructing medium through the use of the Darcy number, Da in the range of 10^{-6} to 1. As can be seen in Fig. 6, at higher values of the Darcy number, the vibrational effect becomes more pronounced. The isotherms for $Da = 10^{-6}$ (Fig. 6a) shows a very thin thermal boundary layer due to the presence of a dominant buoyancy induced flow. As the value of Da increases to 10^{-4}, the buoyancy force becomes weaker leading to a thicker thermal boundary layer as seen in Fig. 6b. This is due to a lower value of Ra when increasing Da for a fixed value of the modified Rayleigh number, Ra_m. As the Darcy number, Da, is further increased, the thermal boundary layer becomes thicker, while the vibrational effect becomes more pronounced leading to a thermally stratified situation and formation of a vortex at the left corner of the cavity as seen in Fig. 6c and d.

5.3. Effect of variations in Ra_m, Re_s, and Da on the heat transfer process

Fig. 7 displays the impact of variations in Ra_m, Re_s, and Da on the average Nusselt number, Nu_{Avg}. As expected at a given Darcy number, an increase in either Ra_m or Re_s enhances the heat transfer across the cavity. It should be noted that when the flow is dominated by natural convection, the average Nusselt number, Nu_{Avg}, increases as the Darcy number decreases for a fixed Rayleigh number, Ra_m. However, when the flow is dominated by vibrational effects, Nusselt number, Nu_{Avg} increases as the Da increases.

5.4. Quantitative and qualitative assessment of different flow regimes and non-Darcian attributes

Nu_{Avg} is used to characterize deviations between using a generalized model with all the effects incorporated and an approximate or a limiting case model. The error in using an approximate or limiting case model, in place of the generalized model, is assessed as follows:

$$Error^{\text{approximate or limiting case model}} = \frac{\left| Nu_{Avg}^{\text{approximate or limiting case model}} - Nu_{Avg}^{\text{generalized model}} \right|}{Nu_{Avg}^{\text{generalized model}}} \tag{16}$$

If the error is below a threshold value of 5%, the difference between the approximate or the limiting case model and the generalized model is considered to be negligible.

Quantitative assessment of different flow regimes based on variations in Re_s, Ra_m, and Da is presented in Fig. 8, while Fig. 9 displays a three dimensional qualitative mapping of these regimes. Four distinct regimes are identified in these figures. These are: conduction dominated, vibration dominated, buoyancy dominated, and mixed convection (vibration-buoyancy) dominated regions. Buoyancy region indicates that within the set of parameters shown in Figs. 8 and 9, the vibrational effect on Nu_{Avg} is less than 5%. Likewise, within the vibration dominated region set by parameters displayed in Figs. 8 and 9, the buoyancy effect on Nu_{Avg} is less than 5%. Within the mixed region, both buoyancy and vibrational effects are important while none of those effects are pertinent in the conduction dominated region. As can be seen, an increase in Da enhances the vibrational effect, while decreasing Da enhances the buoyancy effect.

Additionally, the quantitative assessment of different flow regimes based on variations in Re_s and Ra_m for different values of Pr and dimensionless frequency, γ, are shown in Fig. 10. As can be seen in Fig. 10, the vibration dominated region expands with an increase in the Prandtl number, Pr. On the other hand, an increase in the dimensionless frequency, γ, leads to a shrinkage of the vibration region.

Figs. 11 and 12 illustrate a quantitative assessment and a three dimensional qualitative mapping of non-Darcian attributes, respectively, based on variations in Re_s, Ra_m, and Da. Three basic

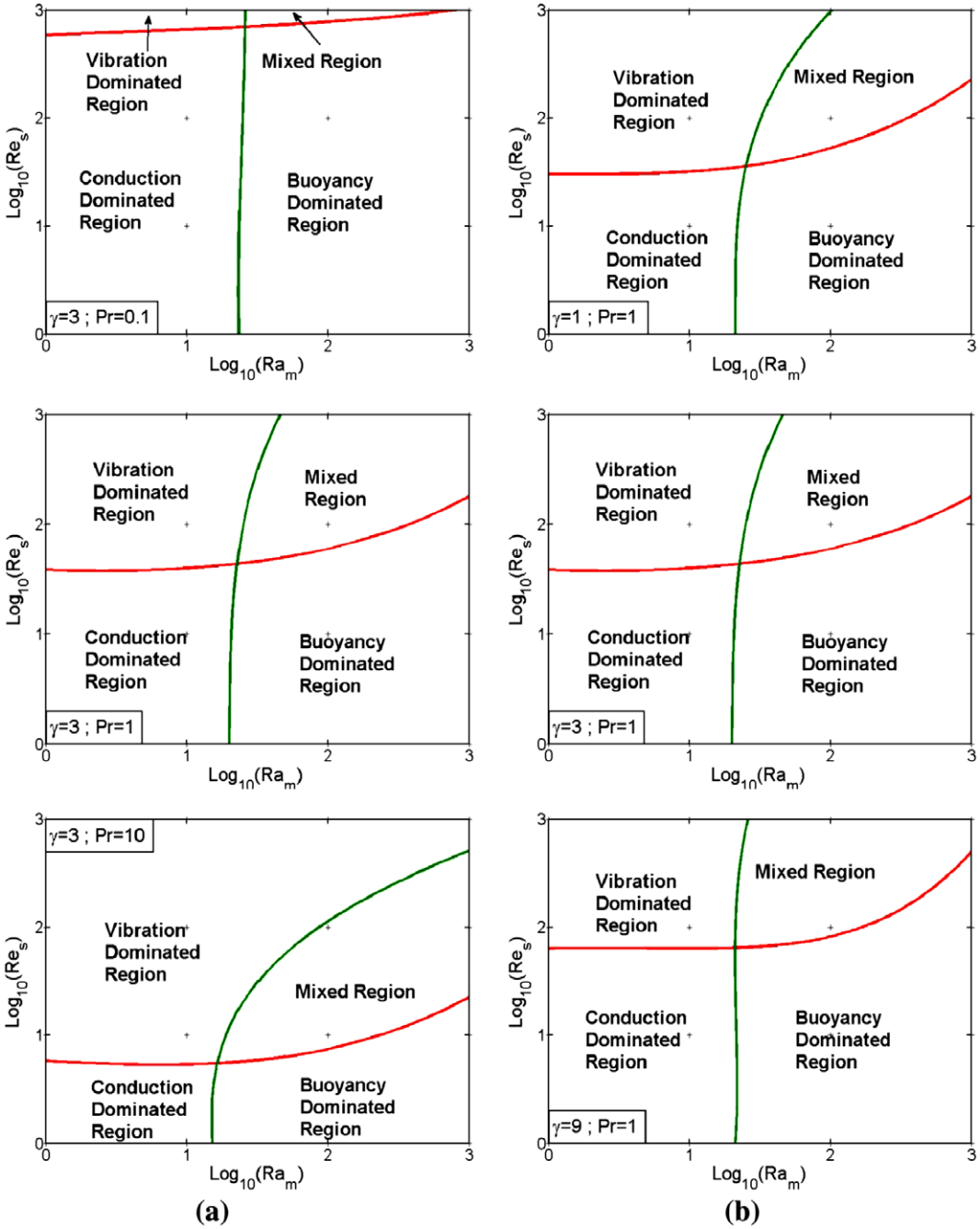

Fig. 10. Quantitative assessment of different flow regions based on variations in Ra_m and Re_s for (a) different values of Pr; (b) different values of γ for $\delta = 0.9$, $\sigma = 1$, $\varepsilon = 4$.

regions are categorized in each figure. These are: a region where the use of Darcy's law produces an error of less than 5%, a region where the generalized equation should be used and a region where the use of regular fluid model produces less than 5% error. As can be seen in Figs. 11 and 12, the generalized region is sandwiched between the Darcian and regular fluid regions. The generalized region expands as the vibrational Reynolds number, Re_s, and modified Rayleigh number, Ra_m, increase. This is due to stronger interaction of the fluid with both the solid boundary and the matrix.

6. Conclusion

Vibrational and buoyancy induced convection in an open-ended obstructed cavity has been investigated in this work. The geometry under consideration is based on a vertical channel with an open-ended top and a vibrating left wall. The computational results for vibrational effects in an unobstructed domain and natural convection in enclosures were validated against earlier works and were found to be in very good agreement. It is shown that increasing Re_s and/or Da enhances the vibrational effect and that high values of Re_s lead to the formation of a vortex. As expected an increase in Re_s and/or Ra_m results in an enhancement in heat transfer, while the effect of Da depends on which of the mechanisms dominates the system.

Effect of the obstructing medium as well as vibration in terms of Re_s, Ra_m and Da on the heat transfer process is demonstrated. It is shown that as the obstructing medium become more permeable, the vibrational effect becomes more substantial leading to formation of a vortex at the left corner of the cavity for larger values of

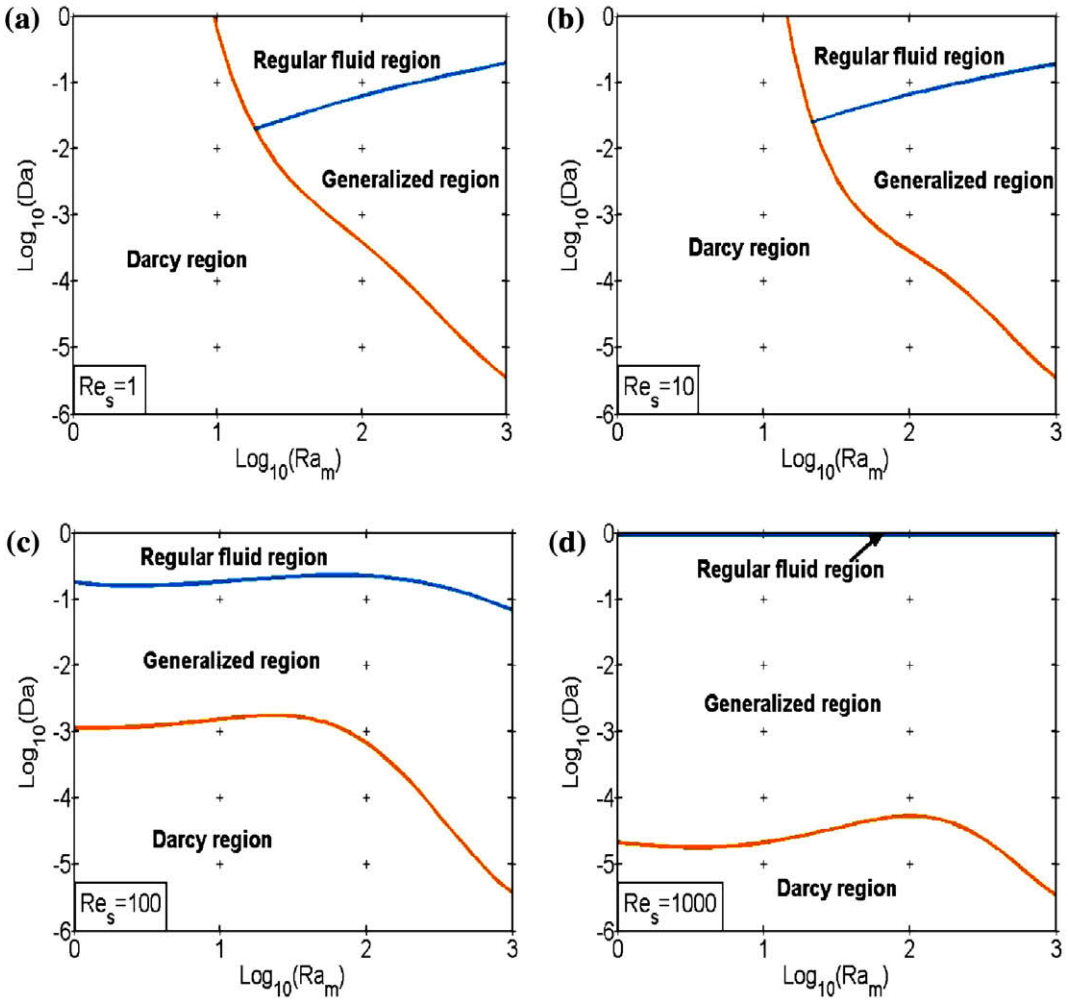

Fig. 11. Quantitative assessment of non-Darcian attributes based on variation in Re_s, Ra_m, and Da (Pr = 1, $\gamma = 3$, $\delta = 0.9$, $\sigma = 1$, $\varepsilon = 4$).

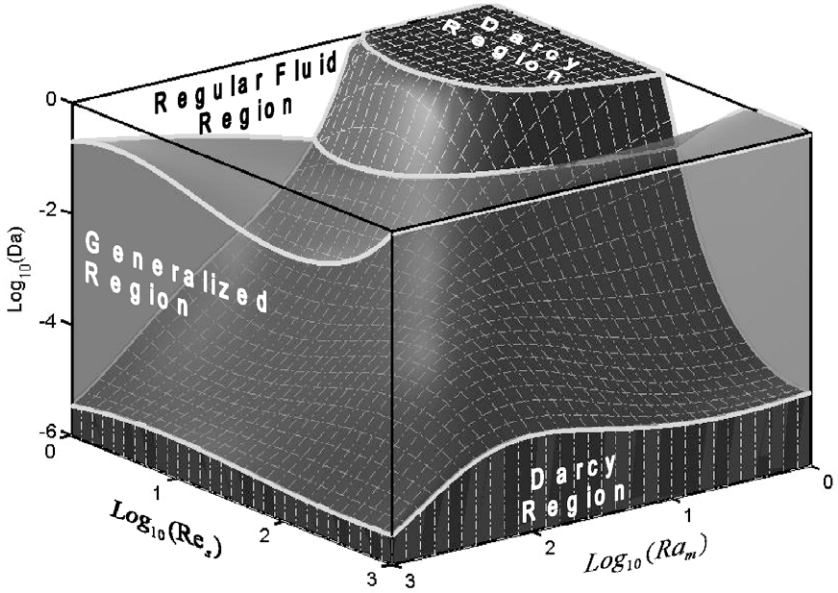

Fig. 12. Three dimensional qualitative mapping of non-Darcian attribution based on variations in Re_s, Ra_m, and *Da* (Pr = 1, $\gamma = 3$, $\delta = 0.9$, $\sigma = 1$, $\varepsilon = 4$).

Re_s. The quantitative and qualitative assessment of different flow regimes and non-Darcian attributes are synthesized and four distinct regimes are identified and characterized in this work. Finally, the qualitative mappings of the non-Darcian attributes are presented through the introduction of three basic regimes. This work constitutes the first study of vibration induced mixed convection in an open-ended obstructed cavity.

References

[1] V. Prasad, A. Tuntomo, Inertial effects on natural convection in a vertical porous cavity, Numer. Heat Transfer 11 (1987) 295–320.
[2] G. Lauriat, V. Prasad, Non-Darcian effect on natural convection in a vertical porous enclosure, Int. J. Heat Mass Transfer 11 (1989) 2135–2148.
[3] M. Karimi-Fard, M.C. Charrier-Mojitabi, K. Vafai, Non-Darcian effects on double diffusive convection within a porous medium, Numer. Heat Transfer A 31 (1997) 837–852.
[4] K. Vafai, H. Hadim, Overview of current computational studies of heat transfer in porous media and their applications – natural convection and mixed convection, in: W.J. Minkowycz, E.M. Sparrow (Eds.), Advances in Numerical Heat Transfer, Vol. 2, Taylor & Francis, New York, 2000, pp. 331–371 (10).
[5] A. Bejan, C.L. Tien, Natural convection in a horizontal porous medium subjected to an end-to-end temperature difference, ASME J. Heat Transfer 100 (1978) 191–198.
[6] M. Haajizadeh, C.L. Tien, Natural convection in a rectangular porous cavity with one permeable endwall, ASME J. Heat Transfer 105 (1983) 803–808.
[7] K. Vafai, C.L. Tien, Boundary and inertia effects on flow and heat transfer in porous media, Int. J. Heat Mass Transfer 24 (1981) 195–203.
[8] A. Amiri, K. Vafai, Transient analysis of incompressible flow through a packed bed, Int. J. Heat Mass Transfer 41 (1998) 4259–4279.
[9] A. Amiri, K. Vafai, Analysis of dispersion effects and non-thermal equilibrium, non-Darcian, variable porosity incompressible flow through porous media, Int. J. Heat Mass Transfer 37 (6) (1994) 939–954.
[10] J. Ettefagh, K. Vafai, Natural convection in open-ended cavities with a porous obstructing medium, Int. J. Heat Mass Transfer 31 (1987) 673–693.
[11] J. Ettefagh, K. Vafai, S.J. Kim, Non-Darcian effects in open-ended cavities filled with a porous medium, J. Heat Transfer 113 (1991) 747–756.
[12] K. Vafai, J. Ettefagh, The effect of sharp corners on buoyancy-driven flows with particular emphasis on outer boundaries, Int. J. Heat Mass Transfer 33 (1990) 2311–2328.
[13] K. Khanafer, K. Vafai, Effective boundary conditions for buoyancy-driven flows and heat transfer in fully open-ended two-dimensional enclosures, Int. J. Heat Mass Transfer 45 (2002) 2527–2538.
[14] K. Khanafer, K. Vafai, M. Lightstone, Mixed convection heat transfer in two-dimension open-ended enclosure, Int. J. Heat Mass Transfer 45 (2002) 5171–5190.
[15] W.S. Fu, W.J. Shieh, Transient thermal convection in an enclosure induced simultaneously by gravity and vibration, Int. J. Heat Mass Transfer 36 (2) (1993) 437–452.
[16] H. Kimoto, H. Ishida, Vibration effects on the average heat transfer characteristics of the natural convection field in a square enclosure, Heat Transfer – Asian Res. 29 (7) (2000) 545–558.
[17] L.A. Florio, A. Harnoy, Use of a vibrating plate to enhance natural convection cooling of a discrete heat source in a vertical channel, Appl. Therm. Eng. 27 (13) (2007) 2276–2293. Heat Powered Cycles-4.
[18] Y.P. Razi, K. Maliwan, M.C. Carrier-Mojitobi, A. Mojitobi, The Influence of Mechanical Vibrations on Buoyancy Induced Convection in Porous Media, in: Handbook of Porous Media, 2005, pp. 321–370.
[19] A.-R.A. Khaled, K. Vafai, Heat transfer and flow induced by both natural convections and vibration inside an open-end vertical channel, Heat Mass Transfer 40 (2004) 325–337.
[20] K. Vafai, Convection flow and heat transfer in variable-porosity media, J. Fluid Mech. 147 (1984) 233–259.
[21] T.S. Lundgren, Slow flow through stationary random beds and suspensions of spheres, J. Fluid Mech. 51 (1972) 273–299.
[22] G. Neale, W. Nader, Practical significance of brinkman's extension of Darcy's law, Canadian J. Chem. Eng. 52 (1974) 475–478.
[23] G.S. Beavers, E.M. Sparrow, Non-Darcy flow through fibrous porous media, ASME J. Appl. Mech. 36 (1969) 711–714.
[24] G. Lauriat, V. Prasad, Natural convection in a vertical porous cavity: a numerical study for Brinkman-extended Darcy formulation, natural convection in porous media, ASME HTD 56 (1986) 13–23.
[25] V. Prasad, G. Lauriat, N. Kladias, Reexamination of Darcy–Brinkman solutions for free convection in porous media, in: Proceeding National Heat Transfer Conference, Houston, vol. 1, ASME, New York, pp. 569–579.